IEEE Access
Multidisciplinary | Rapid Review | Open Access Journal

Received May 4, 2019, accepted May 26, 2019, date of publication May 31, 2019, date of current version June 13, 2019.

Digital Object Identifier 10.1109/ACCESS.2019.2920134

Personalised Control of Robotic Ankle Exoskeleton Through Experience-Based Adaptive Fuzzy Inference

KAIYANG YIN[1,2], KUI XIANG[1], MUYE PANG[1], JING CHEN[1], PHILIP ANDERSON[2], AND LONGZHI YANG[2], (Senior Member, IEEE)

[1]School of Automation, Wuhan University of Technology, Wuhan 430070, China
[2]Department of Computer and Information Sciences, Northumbria University, Newcastle upon Tyne NE1 8ST, U.K.

Corresponding author: Longzhi Yang (longzhi.yang@northumbria.ac.uk)

This work was supported in part by the Fundamental Research Funds for the Central Universities under Grant 2018-JL-003 and in part by the National Natural Science Foundation of China under Grant 61603284.

ABSTRACT Robotic exoskeletons have emerged as effective rehabilitation and ability-enhancement tools, by mimicking or supporting natural body movements. The control schemes of exoskeletons are conventionally developed based on fixed torque-ankle state relationship or various human models, which are often lack of flexibility and adaptability to accurately address personalized movement assistance needs. This paper presents an adaptive control strategy for personalized robotic ankle exoskeleton in an effort to address this limitation. The adaptation was implemented by applying the experience-based fuzzy rule interpolation approach with the support of a muscle-tendon complex model. In particular, this control system is initialized based on the most common requirements of a ''standard human model,'' which is then evolved during its performance by effectively using the feedback collected from the wearer to support different body shapes and assistance needs. The experimental results based on different human models with various support demands demonstrate the power of the proposed control system in improving the adaptability, and thus applicability, of robotic ankle exoskeletons.

INDEX TERMS Robotic ankle exoskeleton, muscle-tendon complex model, adaptive fuzzy rule interpolation, rehabilitation support.

I. INTRODUCTION

The advent of the first active anthropomorphic exoskeleton reported in [1] has led to a booming of developing wearable robotics to support people to achieve different physical tasks. Based on its purposes, exoskeletons can be classified into two groups: assistance and therapeutic devices. Most of the wearable exoskeletons are designed to assist individuals in performing their daily living activities and enhance human mobility [2], [3], whilst only a small number of devices focus on therapeutic effects. Therapeutic devices are often used for body training, in an effort to enhance patients' capabilities affected by neuromuscular injury, such as chronic degenerative low back pain, head injuries, stroke, peripheral neuropathies and cerebral palsy [4]. Upright balance training is one of the activities to help patients retain neuro-sensory and muscular movement function [5]. The efforts required to maintain balance effectively train the muscle activation and movement coordination functions, which are the indispensable process towards the walking ability training stage.

The ankle-foot complex plays an important role in human upright balance control. Balance control ensures a human doesn't fall down when feet are stationed, which involves an intricate dynamic behavior of the lower limbs and their interaction with the floor [6]. In this process, the ankle plantar flexor and dorisiflexor muscles work together to keep the body upright. The lack of ankle functionality led by neuromusclar injury represents a crucial limitation for standing balance. The robotic ankle exoskeleton can support people who suffer from ankle injuries to keep balance when standing, and to train them to regain the ankle function during rehabilitation. Extensive researches have been conducted in understanding the human standing balance strategy from physiology point of view in order to provide better

The associate editor coordinating the review of this manuscript and approving it for publication was Yonghong Peng.

support during rehabilitation and also design and build more advanced ankle exoskeleton robot for standing support [7].

Robotic ankle exoskeleton devices are usually designed and developed by simulating the mechanism of the human body, and the control strategy of such devices are often developed using various sensor measurements [8]–[11]. Ankle stiffness modulation was discovered to be a key factor in human balancing, and a torsional spring-loaded flywheel pendulum was proposed to approximate human body dynamics [12]. In this work, stiffness adjustment was implemented by a common mathematical model, which is lack of flexibility to meet individual's needs. To address this, the stiffness of the ankle joint was varied proportionally to its distance to the limits of stability in the work of [13]. In this case, a scaling factor needs to be provided for each wearer, which is not very practical. Another way to solve the inflexibility issue is the open-loop balance control as proposed in [14], which requires pre-planned joint trajectory. The planned joint trajectory is usually inconsistent with human joint trajectory to some extent, which may cause discomfort to the exoskeleton wearer, or even disturb human balance.

This work proposes an adaptive robotic ankle exoskeleton controller, which is able to adaptively meet different wearers' individual needs. This is implemented by applying the recently proposed experience-based adaptive fuzzy rule interpolation system [15], with the support of a muscle-tendon complex model [16]. Briefly, the experience-based adaptive fuzzy rule interpolation evolves its rule base through an effective revision mechanism based on the performance feedback of the controlled system, to address the issue of lack of labeled data or expert knowledge. Particularly in this project, a fuzzy inference system was initialised based on a typical human model to provide the parameter required by the muscle-tendon model, which works collaboratively as a general control model for the ankle exoskeleton for all wearers. Once the ankle exoskeleton is worn by an individual, the adaptive fuzzy inference system will then adapt the rule base according to the feedback collected from the wearer to meet the wearer's personalized needs. The proposed approach was validated and evaluated through simulations implemented using OpenSim. The experimental results show the working of the proposed control system for robotic ankle exoskeleton in meeting different wearers' personalized needs.

The rest of the paper is organised as follows. Section II reviews the technical background and related works. Section III details the proposed personalized control approach. Section IV reports the experimental results with discussions. Section V concludes the paper and points out important future work.

II. BACKGROUND

The two integral components of the proposed system, including the muscle-tendon complex model and the experience-based adaptive fuzzy inference system, are reviewed in this section.

A. MUSCLE-TENDON COMPLEX MODEL

A typical human ankle joint is driven by two groups of muscles, the plantar flexor muscle group and the dorsiflexor muscle group. The former mainly consists of soleus (SOL) and gastrocnemius (GAS), whilst the latter primarily refers to the tibialis anterior (TIB). Both muscle groups can each be simplified as a muscle-tendon complex (MTC) model, with other related but marginally influenced muscles ignored. The MTC model can be simulated by a combination of a contractile element (CE) and a series elastic element (SEE), as shown in Fig. 1, with the muscle fibers and the tendon represented by the CE and the SEE, respectively. The CE and SEE are connected in series, where the SEE is a non-linear, unidirectional spring representing the Achilles tendon [17].

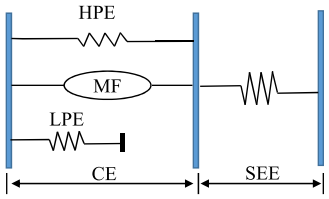

FIGURE 1. The muscle-tendon complex model.

The CE consists of three unidirectional components, including an active Hill-type muscle fibers tissue (MF) [18] with a positive force feedback reflex scheme, a high-limit parallel elastic component (HPE), and a low-limit parallel elastic component (LPE). The optimal length of the MF, denoted as l_{opt}, is equal to the length of the CE when the CE provides the maximum isometric force (F^{max}), i.e., $l_{CE} = l_{opt}$. If the CE stretches beyond its optimal length, i.e., $l_{CE} > l_{opt}$, the HPE engages. That is, the HPE effectively prevents the CE from overstretching. Conversely, the LPE prevents the CE from over-shrinking, if the SEE is unengaged.

1) CONTRACTILE ELEMENT

The active component of a CE is the MF with a positive force feedback reflex scheme which exerts an unidirectional force. The force of the MF (F_{MF}) is determined by the muscle fibers length (l_{CE}), the contraction velocity (v_{CE}), the activation value (a), and the pre-learned maximum muscle fibers force (F^{max}) [16], as expressed below:

$$F_{MF} = aF^{\max} f_l(l_{CE}) f_v(v_{CE}), \tag{1}$$

where $f_l(l_{CE})$ represents the force-length relationship function of the Hill-type muscle model, and $f_v(v_{CE})$ is the force-velocity relationship function of the CE.

The force-length relationship function $f_l(l_{CE})$ is a bell-shaped curve as illustrated in Fig. 2(a), which is defined as [16]:

$$f_l(l_{CE}) = \exp\left[c\left|\frac{l_{CE} - l_{opt}}{l_{opt}\omega}\right|^3\right], \tag{2}$$

where ω denotes the width of the bell-shaped curve, and c represents the curve's magnitude near the extreme of the bell

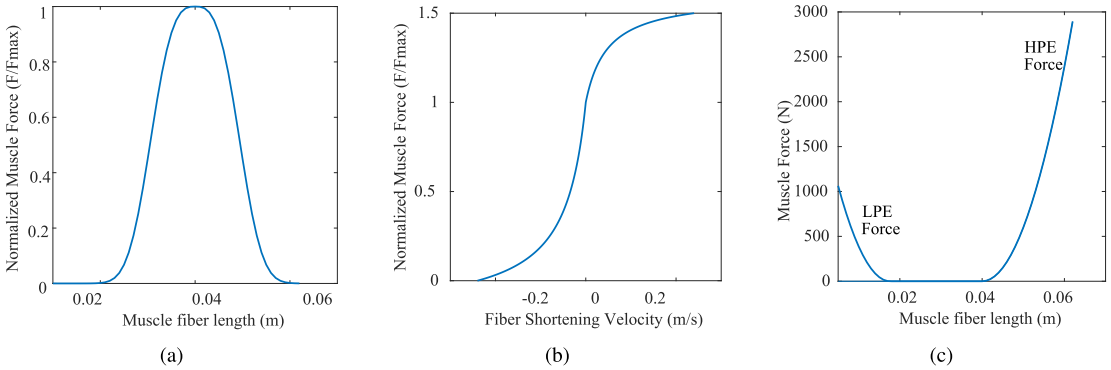

FIGURE 2. Contraction dynamics of a CE for a typical muscle group. (a) Isomeric force fiber length relationship. (b) Isomeric force fiber shortening velocity relationship. (c) Parallel elasticity force fiber length relationship.

(which is defined as $ln(0.05)$ in this work) fulfilling:

$$f_l(l_{CE} = (1 \pm \omega)l_{opt}) = 0.05. \tag{3}$$

The force-velocity relationship function, $f_v(v_{CE})$, of CE follows the Hill equation [18] as illustrated in Fig. 2(a), which is defined by:

$$f_v(v_{CE}) = \begin{cases} (v_{\max} - v_{CE})/(v_{\max} + Kv_{CE}), & v_{CE} < 0 \\ N + (N-1)\dfrac{v_{\max} + v_{CE}}{7.56Kv_{CE} - v_{\max}}, & v_{CE} \geq 0, \end{cases} \tag{4}$$

where v_{max} indicates the maximum contractile velocity of the muscle fibers, K stands for a curvature constant, N describes the dimensionless muscle force which is normalised by F^{max}. The force-length relationship function for HPE is shown in the right side of Fig. 2(c), which is given by [10]:

$$F_{HPE}(l_{CE}) = \begin{cases} F_{\max}[(l_{CE} - l_{opt})/(l_{opt}\omega)]^2, & l_{CE} > l_{opt} \\ 0, & otherwise. \end{cases} \tag{5}$$

The force-length relationship function for LPE is illustrated in the left side of Fig. 2(c), which is expressed as [10]:

$$F_{LPE}(l_{CE}) = \begin{cases} F_{\max}\dfrac{[(l_{CE} - l_{opt}(1-\omega))/l_{opt}]^2}{(\omega/2)}, & l_{CE} \leq l_{opt}(1-\omega) \\ 0, & otherwise. \end{cases} \tag{6}$$

The overall force of CE, i.e., (F_{CE}), is then:

$$F_{CE} = F_{MF}(l_{CE}, v_{CE}, a) + F_{HPE} - F_{LPE}. \tag{7}$$

Since the CE and SEE are connected in series, the following equation holds:

$$F_{CE} = F_{SEE} = F_{MTC}, \tag{8}$$

where the F_{SEE} denotes the force of the SEE and F_{MTC} represents the force of the entire MTC.

2) SERIES ELASTIC ELEMENT

The SSE operates as a tendon which is connected in series with the CE as introduced above. The SEE can be described as a nonlinear spring:

$$F_{SEE} = \begin{cases} F_{\max}(\varepsilon/\varepsilon_{ref})^2, & \varepsilon > 0 \\ 0, & \varepsilon \leq 0, \end{cases} \tag{9}$$

where ε is the tendon strain, and ε_{ref} is the reference tendon strain as $F_{SEE} = F_{max}$ when $\varepsilon > 0$. As reported in [14], this quadratic form was used as an approximation of the commonly-modeled piecewise exponential-linear tendon stiffness curve, to reduce the number of the model parameters. In particular, the tendon strain is defined as:

$$\varepsilon = \frac{l_{SSE} - l_s}{l_s}, \tag{10}$$

where l_{SSE} is the length of the SSE, and l_s is the resting length of the tendon.

3) POSITIVE FEEDBACK REFLEX SCHEME

The MF activation value (i.e., a) of the CE can be generated by the positive force feedback reflex scheme [10], [16], [19]. Denote the signal-propagation time delay as Δt. The current stimulation of MF, $(S(t))$, at any time before Δt is S_0; otherwise, $S(t)$ equals to the pre-stimulation (S_0) plus the production of the CE force (F_{CE}) at time $(t - \Delta t)$ and a reflex gain (G). $S(t)$ can then be expressed as:

$$S(t) = \begin{cases} S_0, & t < \Delta t \\ S_0 + GF_{CE}(t - \Delta t), & t \geq \Delta t, \end{cases} \quad 0 \leq S(t) \leq 1. \tag{11}$$

The stimulation is low-pass filtered with a constant of time to simulate the muscle excitation-contraction coupling. The resulting signal is constrained to the range between 0 and 1, which is used as the MF activation value (a) in Eq. 1.

B. FUZZY INFERENCE

Fuzzy inference is the process of formulating the mapping from an input space to an output space using fuzzy logic

which is able to represent non-linear, high dimensional, and vague models using fuzzy rule bases representing the knowledge. The rule bases are generated using prior knowledge which can be either human expertise or labelled training data instances [20], [21]. Due to the sparsity and imbalanced distribution of expert knowledge or labelled training data samples, the generated rule bases may be sparse at some parts of the problem domain. In this case, conventional fuzzy inference systems will fail to generate any conclusions for the inputs that are not covered by the rule bases. Fuzzy rule interpolation (FRI) was developed to address this limitation [22]–[25].

FRI is a generalization of crisp linear interpolation under the uncertainty representation framework of fuzzy logic. Given an input that does not overlap with any rule antecedent due to the sparseness of rule bases, the two closest neighboring rules are selected based on a given fuzzy distance metric for interpolation or extrapolation. If the widely applied transformation-based interpolation approach [25] is used, an intermediate rule is generated first such that its antecedent representation value is as âĂIJcloseâĂİ to the given input as possible. From this, a conclusion is derived by ensuring the shape distinguishability between the conclusion and the consequence of the intermediate rule is equal to that between the antecedents of the interpolated rule and intermediate rule. In addition to being able to work with sparse rule bases, FRI can also reduce system complexity if the fuzzy model is too complex. FRI approaches have been further developed from different perspectives, such as, rough-FRI [26], dynamic version of FRI [27], adaptive FRI [22], [28], [29], and experience-based FRI [15].

The experience-based FRI (E-FRI) is able to adapt to different applications with limited human expert knowledge or labelled training data instances, which is thus applied in this work. In particular, the system first initialises the rule base, for a given application, with a very limited number of rules representing the incomplete, or standard system knowledge based on the most common model. A typical single input and single output rule R_i is of the following format:

$$R_i : \textbf{IF } x \textit{ is } A_i, \textbf{ THEN } y \textit{ is } B_i \ (w_i, EF_i, \tag{12}$$

where A_i and B_i are fuzzy sets, w_i stands for the inherent weight of the rule expressing its confidence degrees, EF_i is the experience factor representing the usage and effectiveness information of the rule during the performance, CD_i is the cooling down factor indicating the timeliness of the rule.

The importance factor IF of each rule, regarding a given input, can be calculated as a function of the weight and the distance between the input and the existing rule antecedents using:

$$IF_i = \sqrt{\frac{1/d_i}{\sum_{i=1}^{n} 1/d_i}} w_i, \tag{13}$$

where, d_i is the defuzzified distance between the input and rule antecedent, w_i represents the weight of the rule, n is the number of rules in the existing rule base. By this equation, the two most ''informative'' rules are selected for FRI to generate the output.

The rule base evolves whilst it performs inferences by a revision mechanism. Specifically, the historic inference performance indicators are used to provide the system the experience feedback to determine the inherent weights of rules, in addition to the timeliness information to avoid the inclusion of too many out of date rules. Based on the feedback, three types of revisions effectively ensure the conciseness, timeliness, effectiveness, and efficiency of the rule base, including updating the weights of existing rules, removing useless rules, and adding new rules. More technical details of the E-FRI can be found in [15].

III. PERSONALIZED CONTROL OF ROBOTIC ANKLE EXOSKELETON

The proposed personalized control system is able to learn to adapt whilst it performs, and thus the controlled exoskeleton is expected to work better along time through control system evolving. Following an overall overview of the system, the two key components of the control system, including the control of the simulated muscle actuator and system adaptation through the experience-based FRI are detailed in this section.

A. SYSTEM OVERVIEW

The overall architecture of the robotic ankle exoskeleton system with the proposed personalized control system is illustrated in Fig. 3. The robotic ankle exoskeleton is driven by two actuators that simulate the effects of the two groups of muscle in the ankle, including the plantar flexor muscle group and the dorsiflexor muscle group, as introduced at the beginning of Section II-A. The working mechanism of these actuators for robotic ankle exoskeleton is detailed in Section III-B. The control signals of these actuators are generated through the MTC model as discussed in Section II-A, with its parameter adaptively adjusted by the E-FRI as detailed in Section III-C.

The data flow in the interconnected closed control loops guarantees the strong adaptability of the proposed control approach. The inputs of the MTC model are calculated using the Geometric Attachment component based on the current state of the exoskeleton ankle; the inputs include the length of MTC (l_{MTC}), the length of CE (l_{CE}), the fiber contraction velocity (v_{CE}), and the moment arm of MTC force (r_{arm}). The output of the MTC is the flexor torque (T_{flexor}) based on its parameters provided by the E-FRI, which is then passed to the torque actuator component to drive the exoskeleton to perform the next action. The rule base of the E-FRI system was initialised based on a ''standard human'' model, which is then evolved using the performance feedback of the ankle exoskeleton from the actual wearer; the feedback can be collected in multiple ways, such as through electromyography [30], but this is out of the scope of this paper.

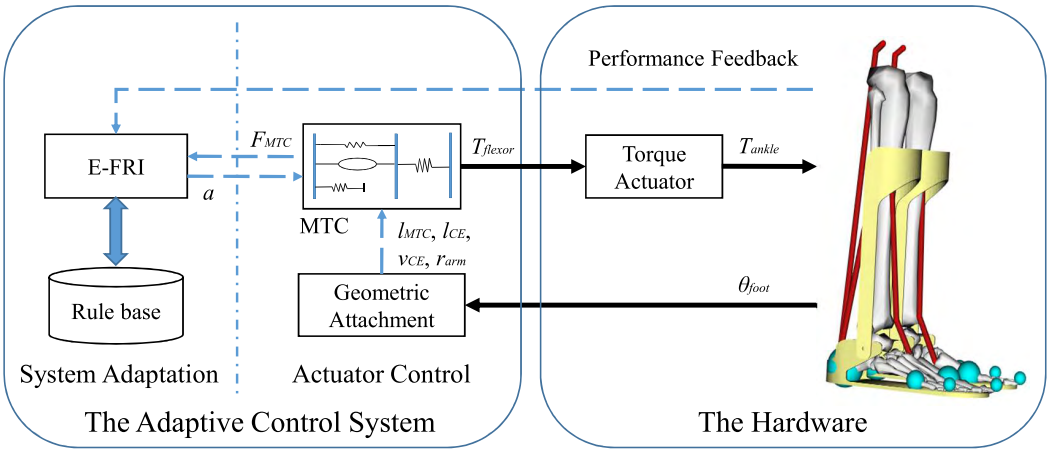

FIGURE 3. The overview of the proposed personalised control architecture.

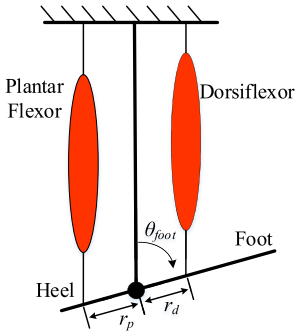

FIGURE 4. The geometry of an exoskeleton including the angle between the variable moment arm and the ankle for the MTC model.

B. ACTUATOR CONTROL

The two simulated flexor muscle actuators are illustrated in Fig. 4. The force of these simulated muscle groups can be calculated using Eqs. 1, 7, and 8, from the muscle activation, the length of MF in the CE, and its contraction velocity. The results are then used to compute the ankle torque to drive the torque actuator. The muscle activation value is determined by the E-FRI which is detailed in the next subsection. The length of the MF in the CE and the fiber contraction velocity can be computed using the robotic exoskeleton ankle angle θ_{foot}, which is defined as the angle between the foot and the shank segment, as illustrated in Fig. 4. In particular, the length of the MTC (l_{MTC}) is computed as [10]:

$$l_{MTC} = r\rho(\sin(\theta_{foot} - \theta_{\max}) - \sin(\theta_{ref} - \theta_{\max})) + l_s + l_{opt}, \tag{14}$$

where r is the attachment radius of plantar flexor muscle and dorsiflexor muscle, ρ is a scaling factor representing the pennation angle of the muscle fibers, θ_{ref} is the ankle reference angle at which $l_{CE} = l_{opt}$, and θ_{max} is a constant ankle angle value subject to $max(r_{arm}) = rcos(\theta_{foot} - \theta_{\max})$ with (θ_{foot}) being the robotic exoskeleton ankle angle.

The MF length can be calculated by:

$$l_{CE} = l_{MTC} - l_{SSE}, \tag{15}$$

where l_{SSE} is the length of SSE as calculated using Eq. 10. The muscle fiber contraction velocity can be obtained via the differentiation of muscle fiber length. From this, the force of MTC, i.e., F_{MTC}, can by calculated using Eqs. 7 and 8. The relationship between F_{MTC} and the resulting flexor contribution to flexor torque T_{flexor}, is given by:

$$T_{flexor} = F_{MTC} r_{arm}. \tag{16}$$

The MTC model is generally a dynamical system mapping from a single input θ_{foot} to a single output T_{flexor}, through which the torque demand for the plantar flexor muscle group, i.e., T_P and the dorsiflexor muscle group, i.e., T_D can be calculated. From this, the overall ankle torque, T_{ankle}, in the sagittal plane is obtained as the summation of these two torques:

$$T_{ankle} = T_P + T_D. \tag{17}$$

C. SYSTEM ADAPTATION

The MTC model can adapt to different body shapes with various support needs by changing its parameter, i.e, the MF activation value. This is achieved by employing the E-FRI in this work through the muscle force positive feedback reflex scheme. The framework of the adapted E-FRI is shown in Fig. 5, which comprises of mainly three parts: 1) rule base initialization, 2) fuzzy rule interpolation, and 3) rule base revision. In particular, the rule base is initialized based on a small set of data collected using the MTC based on a typical human model. The transformation-based (T-based) FRI is particularly applied in this work to perform FRI inference due to its effectiveness [15], [25], [31]–[33] for muscle activation estimation. Upon deployment, the rule base is constantly revised by a rule base revision mechanism whilst the ankle exoskeleton performs to provide extra moving assistance. The implementation of these three main components of the

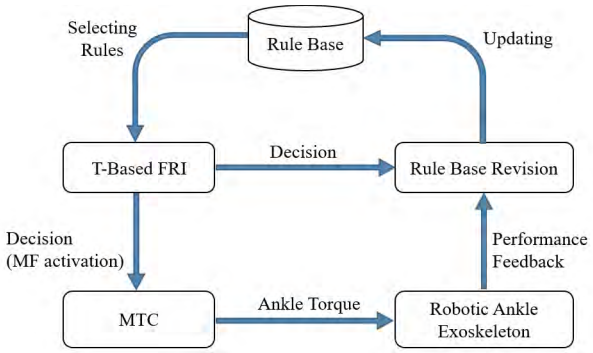

FIGURE 5. Adaptive MTC parameter generation through experience-based fuzzy interpolation for personalized ankle exoskeleton control.

adaptive E-FRI for personalized ankle exoskeleton control are detailed in the following subsections.

1) RULE BASE INITIALISATION

The rule base is initialised with a data set collected from a human upright balance keeping experiment based on a typical human model. Each rule in the rule base is of the form as expressed in Eq. 12, where the input x represents the MTC force (F_{MTC}) provided by the MTC model, and the output y is the MF activation value (i.e., a). For simplicity, triangular membership functions are employed in this work to represent fuzzy sets. EF is initialised based on empirical experience; generally, a large EF value leads to a longer convergence time, and a smaller EF value may result to unexpected rule removal. CD is initialised as 0. These two factors jointly determine the inherent weight of the corresponding rule by:

$$w = \left(\frac{2}{1+e^{-\frac{EF}{n}}} - 1\right)\left(1 - \frac{1}{1+5e^{-\frac{CD}{a}+b}}\right), \tag{18}$$

where a, b, n are sensitivity factors. The values of these factors are empirically determined in this work.

Note that the initialized rule base only works optimally for the "typical human model" used in the data collection process, and the needs from different wearers vary. Therefore, the rule base needs to be adaptively revised as discussed in Section III-C.3 when the fuzzy model performs inferences as detailed in Section III-C.2 below.

2) T-BASED FUZZY RULE INTERPOLATION

Given a MTC force demand (F_{MTC}) represented by fuzzy set A^*, the most "informative" rules regarding this demand in the rule base can be identified using Eq. 13, to support the interpolation inference. Suppose the selected rules for interpolation are R_i and R_j, and denote the interpolated result as B^*. An intermediate rule R^*, "**IF** x *is* $A^{*\prime}$, **THEN** y *is* $B^{*\prime}$" is interpolated first using analogy-based reasoning [34], [35], where the $A^{*\prime}$ and A^* share the same representative value [24]. From this, the shape difference between the given input A^* and the antecedent of intermediate rule $A^{*\prime}$ can be calculated using a transformation metric, which can be implemented in multiple ways as reported in the literature [36]. In particular, the scale and move transformation-based approach [37], [38] is applied in this work due to its wide application. Once the scale rate (S) and move transformation rate (M) are calculated, the corresponding consequence B^* can be computed by applying S and M to the consequence of the intermediate rule $B^{*\prime}$. After deffuzification, the consequence is then sent to the MTC, in addition to the information from the Geometric Attachment component as shown in Fig. 3, for actuator torque calculation, which in turn drives the exoskeleton to provide body movement support to the wearer.

3) RULE BASE REVISION

Note that the performance of the exoskeleton may not be accurately suitable for the wearer as the original system is developed based on a "typical human model" and the wearer's need may change over time. In the proposed adaptive control system, the rule base keeps being revised based on the performance feedback whilst the control system performs fuzzy inferences. There are three types of revisions, including updating the weights of existing rules, removing useless rules, and adding new rules. In specific, if a rule has been selected to perform the T-Based FRI and the performance feedback is positive, the EF value of this rule will be increased by 1 and the CD value will be reset to 0; otherwise, if the performance feedback of the selected rule is negative, the EF value will be decreased and the CD value will be reset to 0. In the meantime, the CD values of all the unused rules will be increased by 1, and their EF value will remain the same. Accordingly, the inherent weight of each rule in the current rule base will be updated utilizing Eq. 18.

Suppose that there are n rules $\{R_1, R_2, \cdots, R_n\}$ in the existing rule base, and the interpolated rule is R^*, the rule base revision process is summarised in Fig. 6. When a new interpolated rule R^* is generated, the similarity degree between each rule in the existing rule base and the interpolated rule is calculated. Suppose that the interpolated rule R^* is "**IF** x *is* A^*, **THEN** y *is* B^* (w^*, EF^*, CD^*)", and an existing rule R_i ($1 \leq i \leq n$) is "**IF** x *is* A_i, **THEN** y *is* B_i (w_i, EF_i, CD_i)". The similarity degree between the two rules, $S(R_*, R_i)$, can be calculated as:

$$S_i = \frac{S(A_i, A^*) + S(B_i, B^*)}{2}, \tag{19}$$

where $S(A_i, A^*)$ and $S(B_i, B^*)$ indicate the similarity degrees between the antecedents and the consequences of the interpolated rule R^* and the existing rule R_i, respectively. There are many approaches available for similarity degree calculation between fuzzy sets [39]. In this work, the degrees of similarity between two triangular fuzzy sets $A^* = (a_1^*, a_2^*, a_3^*)$ and $A_i = (a_{i1}, a_{i2}, a_{i3})$ are calculated as:

$$S(A_i, A^*) = 1 - \frac{|a_{i1} - a_1^*| + |a_{i2} - a_2^*| + |a_{i3} - a_3^*|}{|a_{i1} - a_{i3}|}. \tag{20}$$

The similarity degree between two fuzzy sets B^* and B_i can be calculated in the same way.

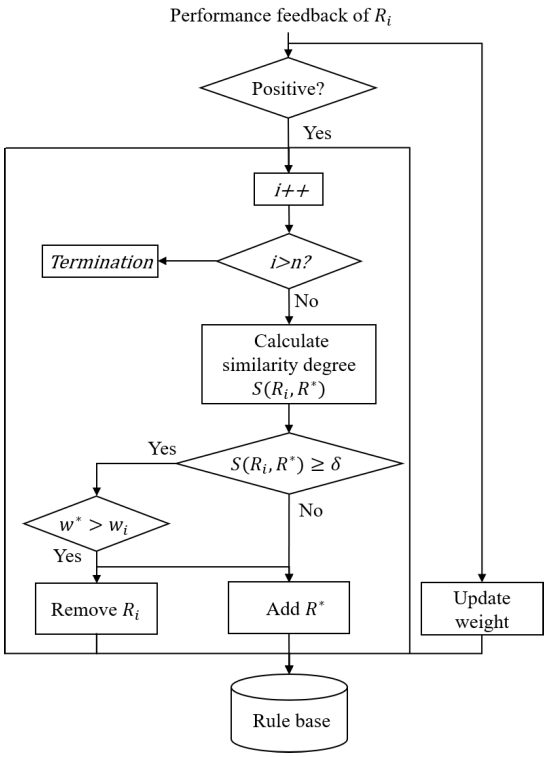

FIGURE 6. The flowchart of rule base revision.

The value of i in Fig. 6 is initialised as 0. Note that Fig. 6 can be optimised for better efficiency during implementation (as R^* may be added for multiple times based on the procedure presented in Fig. 6), but Fig. 6 is employed here to facilitate the description. If the interpolated rule is proven negative based on the performance feedback collected from the wearer, the interpolated rule will be discarded and the weights of the rules in the rule base will be updated. Otherwise, based on a pre-defined similarity degree threshold δ, there are two potential actions in addition to weight updates: 1) if there is not any similar rule in the existing rule base based on Eq. 20, the interpolated rule will be added into the rule base; 2) if there are similar rules but their inherent weights are smaller than that of the interpolated rule, the similar rules in the rule base will be removed whilst the interpolated rule will be added into the rule base; otherwise, the interpolated will be discarded and no extra action is required. This rule base revision mechanism ensures that only the most accurate and timely important rules are included in the rule base, such that the rule base is concise to lead to good performance based on the wearer's personalized and also possibly changing needs.

IV. EXPERIMENTATION

The proposed adaptive control system was applied to a robotic ankle exoskeleton mounted on different human models with various assistance needs for standing balance control and upright control on a moving vehicle for system validation and evaluation. A common simple version of the robotic ankle exoskeleton comprising of two links connected by a rotary joint was used in the experimentation, as shown in Fig. 7(b). The ankle exoskeleton was driven by two actuators to simulate the two group of muscles as introduced in the beginning of Section II-A. The exoskeleton was mounted to the human model's ankle as illustrated in Fig. 7(c) in order to provide movement support for the wearer.

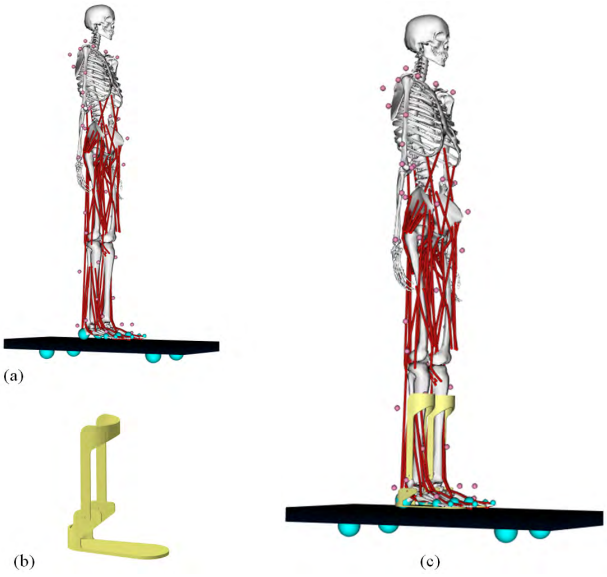

FIGURE 7. Simulated human models and the robotic ankle exoskeleton (a) The humanoid musculoskeletal model. (b) The robotic ankle exoskeleton. (c) The exoskeleton mounted on the human model.

In order to facilitate the experiments, a ''standard human'' model with the most typical body shape and a ''varied human'' model with different body shape were constructed using the OpenSim platform with all the data processed using Matlab. Briefly, the OpenSim is an open source platform for modelling, simulating, and analysing musculoskeletal systems [40]. It supports the construction of the musculoskeletal model with motion visualisation, as illustrated in Fig. 7(a), in addition to extracting meaningful information by a set of integrated tools. Therefore, both actuators of the exoskeleton were also simulated using the OpenSim platform.

A. HUMAN MODEL CONSTRUCTION

To facilitate the verification of the proposed exoskeleton control system, two human models were constructed. In particular, the 12 segments, 29 degree-of-freedoms (DOF) generic musculoskeletal model [41] was adopted as the ''typical human'', which is denoted as Standard Human Model, as shown in Fig. 7(a). From this, a further different human model was also constructed by reconfiguring the anthropometric parameters of the generic model based on the work of [42], which is denoted as Variant Model and used for verify the adaptability of proposed control system. The parameters of these modules are listed in Table 1, where 'COM' stands for the vertical position of the center of human body mass.

TABLE 1. Parameters of human models.

Human model	Weight (kg)	Height (m)	COM vertical (m)
Standard Model	70	1.71	1.06
Variant Model	90	1.88	1.13

The standing balance ability and upright balance ability on a moving vehicle of the ''standard human'' model were tested to ensure the working of the constructed human models, which were also used to initialise the rule base of the proposed adaptive control system. Recall that the human ankle is comprised of soleus (SOL), gastrocnemius (GAS), and tibialis anterior (TIB), as introduced in the beginning of Section II-A. As a common practice, three MTCs were used to function these muscles, with their parameters listed in Table 2.

TABLE 2. Parameter of MTCs for the Standard Human Model.

SOL		GAS		TIB	
variable	value	variable	value	variable	value
S_0^{sol}	0.01	S_0^{gas}	0.01	S_0^{tib}	0.01
G_{sol}	1.6	G_{gas}	1.4	G_{tib}	1.3
$F_{max}^{sol}(N)$	4000	$F_{max}^{gas}(N)$	1500	$F_{max}^{tib}(N)$	3000

1) HUMAN MODEL UPRIGHT BALANCE CONTROL ON A STATIC PLATFORM

In this simulation, the humanoid musculoskeletal reported in [41], that is the Standard Human Model, was implemented. The human model was not standing stable in the beginning when the feet started to take control of the body upright whilst other support for the body was removed. As shown in Fig. 8, after a lean forward to about $-4.8°$, and then lean backward to about $-2.0°$, the body gradually stabilised at around $-2.9° \sim -2.8°$ which is consistent with the research results regarding the human upright equilibrium position as reported in the work of [43].

The simulated ankle torque requirement and the corresponding MTC forces implementing such torque, along the timeline are summarised in Fig. 8. At the initial stage of the simulation, the tilt forward was corresponding to the equilibrium position with the unbalanced force form the sole. In this case, the change of the humanoid gravity produced the forward rotation torque, and the ankle flexor muscle simulator produced the backward rotation torque. That is, the MTC force of SOL and GAS were increased and the MTC force of TIB was decreased. These factors jointly impact the sole's imbalanced force to restore the body to the equilibrium position.

2) HUMAN MODEL UPRIGHT BALANCE CONTROL ON A MOVING VEHICLE

This simulation was the continuation of the first simulation, with the extra condition that the platform was a moving vehicle. The vehicle was given a $1.5m/s^2$ acceleration at time point 5s for 0.1s and the vehicle maintained the speed of $0.15m/s$ until time point 9s; this is followed by a -$1.5m/s^2$ acceleration for 0.1s, and the vehicle returned to its static state. In this simulation, the main balance disturbance was the vehicle acceleration which produced a passive force to the human body.

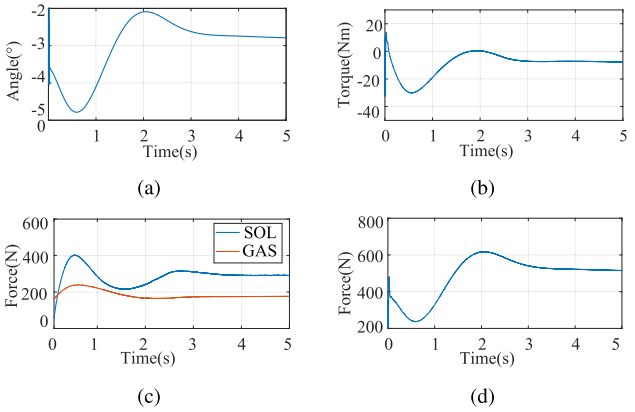

FIGURE 8. Simulation of human upright balance control on the static platform. (a) Human body tilt angle. (b) Ankle torque. (c) MTC force of SOL and GAS. (d) MTC force of TIB.

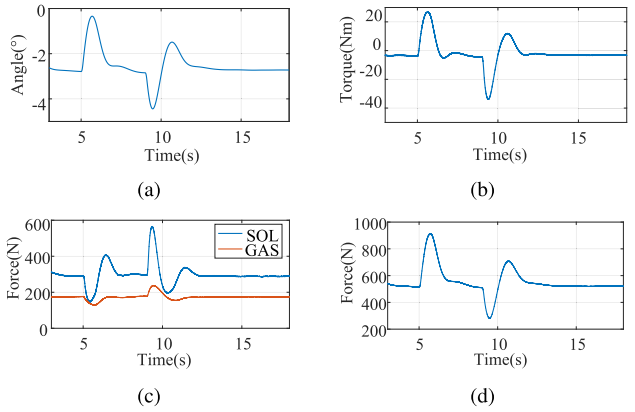

FIGURE 9. Simulation results of human upright control on the moving vehicle. (a) Human body tilt angle. (b) Ankle torque. (c) MTC force of SOL and GAS. (d) MTC force of TIB.

The human body tilt angle, MTC forces, and ankle torque are illustrated in Fig. 9. When the vehicle was imposed a positive forward acceleration at time point 5s, the body leaned backward, compared with the equilibrium position, about $-0.3°$. The corresponding change of humanoid gravity led to some backwards rotation torque, and the ankle flexor muscle simulator reacted on this by producing appropriate forward rotation torque. That is, the MTC forces of SOL and GAS were decreased and the MTC force of TIB was increased. In contrast, when the vehicle was provided a negative acceleration at time point 9s, the body leaned forward, in reference to the equilibrium position, to about $-4.5°$. In this case, the ankle flexor muscle simulator produced backward rotation torque to reflect on the forward rotation torque led by the humanoid gravity change. That is, the MTC force of SOL and GAS were increased and the MTC force of TIB was decreased. These factors jointly restored the body to

TABLE 3. The Initialised rule base.

E-FRI	i	A_i	B_i	w_i	EF_i	CD_i
PMG-FRI	1	$(0, 80, 160)$	$(0.01, 0.03, 0.05)$	0.124	200	0
	2	$(240, 320, 400)$	$(0.07, 0.09, 0.11)$	0.124	200	0
	3	$(640, 720, 800)$	$(0.18, 0.20, 0.23)$	0.124	200	0
DMG-FRI	1	$(0, 80, 160)$	$(0.01, 0.04, 0.07)$	0.124	200	0
	2	$(240, 320, 400)$	$(0.10, 0.13, 0.16)$	0.124	200	0
	3	$(640, 720, 800)$	$(0.26, 0.29, 0.32)$	0.124	200	0

the equilibrium position. The tilt angle of the body finally stabilised at around $-2.9° \sim -2.8°$.

During the above human model construction and experimental task simulation, a small data set was also collected, which was used for the initialisation of the rule base for the E-FRI of the proposed control system as detailed in the next sub-section.

B. EXOSKELETON FOR THE STANDARD HUMAN MODEL

As detailed in Section III-B, two MTC models are used in this work to simulate the plantar muscle group and the dorsiflexor muscle group, whilst the MF activation values fo the MTC models are estimated by the E-FRI in an effort to meet different individual's needs. For convenience, the E-FRI for plantar muscle group is denoted as PMG-FRI, and that for the dorsiflexor muscle group is denoted as DMG-FRI in this work. The MTC models can be readily set up based on the parameters of the constructed human models and the experimental environments as detailed in the last sub-section. The inference mechanism of the E-FRI is detailed in Section III-C, and thus the focus of this section is the construction and the evolving of the fuzzy rule base.

With the support of the data set collected during human model construction and experimental environment simulation as introduced in the last subsection, three initial rules were learned to form the initial rule base for PMG-FRI, and three other rules for DMG-FRI, which are all in the format of Eq. 12. Through empirical study, the experience factor of all rules were initially configured as 200, the cooling down factor were initialised as as 0, the similarity threshold was set as 0.7. From this, the weight of each rule was updated using Eq. 18, and in this experimentation, the parameters of E-FRI were valued as $n = 800$, $a = 100$ and $b = 6$. The rules in the initialised rule base are summarised in Table 3, which are extracted using the domain knowledge of the MTC models.

Based on this rule base, the proposed system can perform control tasks for a robotic ankle exoskeleton. Note that, despite the generality, the simple initialised rule base was not able to produce a highly accurate performance, but the proposed system is able to evolve the rule base while it performs for better performance. To validate this functionality, the initialised controller was applied to perform the simulated upright control tasks as discussed in Section III-A. The feedback from the wearer is usually not available immediately after the performance; therefore, the rule base revision process only occurs once the feedback becomes available. The rule base will be stabilized after a number of performance iterations unless the wearer or the support demand is changed (which will be discussed in the next sub-section). After 5000 inference performances the system rule base stablised with 70 rules.

Take the PMG-FRI as an example for the description of the inference process. A random snapshot of the rule base is summarised in Table 4, given the next input of observed MTC force 385N, the process of inference performance and rule revision are summarised below:

TABLE 4. The random snapshot of the evolved rule base for plantar flexor MTC model of "Typical Human".

i	A_i	B_i	w_i	EF_i	CD_i
1	$(16, 82, 129)$	$(0.014, 0.031, 0.043)$	0.129	208	46
2	$(56, 121, 168)$	$(0.024, 0.041, 0.053)$	0.128	207	43
3	$(89, 154, 201)$	$(0.033, 0.049, 0.062)$	0.112	180	40
4	$(128, 193, 240)$	$(0.043, 0.060, 0.072)$	0.126	203	36
5	$(176, 242, 289)$	$(0.056, 0.073, 0.085)$	0.127	204	33
6	$(333, 409, 447)$	$(0.097, 0.117, 0.129)$	0.125	202	5
7	$(368, 389, 448)$	$(0.107, 0.113, 0.129)$	0.133	214	5
8	$(448, 513, 560)$	$(0.127, 0.148, 0.161)$	0.121	195	12
9	$(524, 552, 622)$	$(0.151, 0.159, 0.179)$	0.134	216	7
10	$(655, 683, 753)$	$(0.188, 0.196, 0.216)$	0.127	204	0

Step 1: Fuzzify the input as fuzzy set $A^* = (340, 390, 425)$.

Step 2: Select the two most "informative" rules for interpolation using Eq. 13. In this case, R_6 and R_7 were selected.

Step 3: Interpolate the rule. The parameters are: relative placement factor $\lambda = -1.43$, the move rate $m = 0.32$, and the scale rate $s = 0.53$. From this, the resulted interpolated rule is: "**IF** *x is* (340, 390, 425), **THEN** *y is* (0.099, 0.113, 0.123)".

Step 4: Defuzzify the consequence $B^* = (0.099, 0.113, 0.123)$ to crisp value 0.112, which was then passed to the MTC as its MF activation value.

Step 5: Generate the torque value by the MTC based on the parameter value and other inputs from the Geometric Attachment component, and apply the torque to the ankle exoskeleton to performance movement assistance.

Step 6: Revise the rule base based on performance feedback. In this case, the feedback was positive. Thus the experience factors of rules R_6 and R_7 were incremented; the cooling down factors reset to 0; the cooling down factor of all other rules decremented, and the weight of all rules updated using Eq. 18.

Step 7: The experience factor of the newly interpolated rule was 198 and the cooling down value was

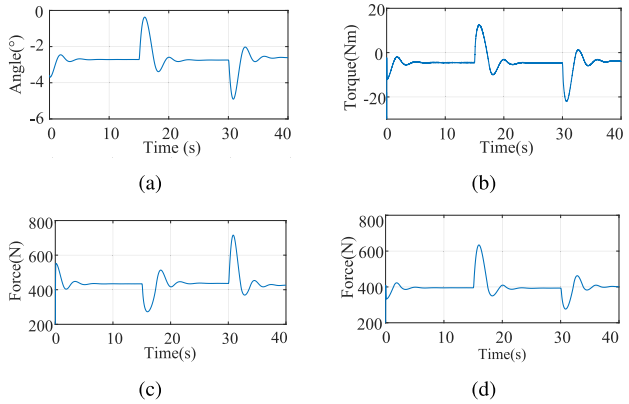

FIGURE 10. Simulation results of the robotic ankle exoskeleton based on the Standard Human Model. (a) Body tilt angle. (b) Ankle torque. (c) Plantar Flexor MTC Force. (d) Dorsiflexor MTC Force.

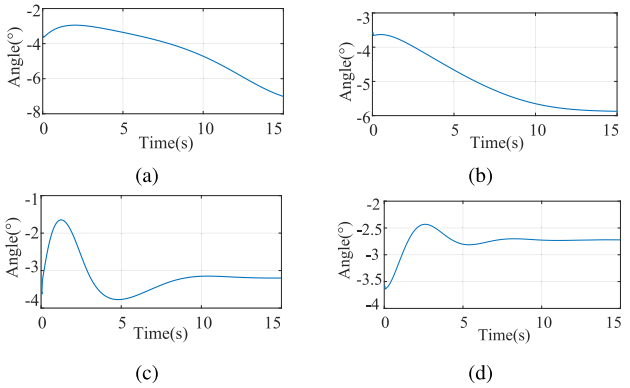

FIGURE 11. The tilt angle evolving along with rule base adaptation. (a) The "standard" rule base. (b) Evolved rule base after 2000 performance iterations. (c) Evolved rule base after 4000 performance iterations. (d) Evolved rule base after 6000 performance iterations.

reset as 0; accordingly, the rule weight was initialised as 0.124 using Eq. 18. The maximum similarity degree between each rule in the existing rule base and the interpolated one was 0.63, which is smaller than the pre-defined threshold 0.7. Therefore, the interpolated rule is added into the existing rule base as: "**IF** *x is* (340, 390, 425), **THEN** *y is* (0.099, 0.113, 0.123) (0.124, 198, 0)."

In order to extend the evaluation of the proposed system, the experiment was also conducted on a moving vehicle. In particular, the vehicle was provided with a $1.5m/s^2$ acceleration for 0.1s at the 15s time point, and the vehicle maintained the speed of $0.15m/s$ until 30s time point, which was followed by a -$1.5m/s^2$ acceleration for 0.1s leading the vehicle to the static state.

The experimental results regarding human body tilt angle, flexor MTC force and the ankle torque is illustrated in Fig. 10. The wearer leaned forward approximately $-3.7°$, and robotic ankle exoskeleton assisted the wearer to lean backwards to about $-2.5°$, and then gradually stabilised at around $-2.9° \sim -2.8°$. When the vehicle was imposed a positive forward acceleration at time point 15s, the body leaned backward, compared with the equilibrium position, about $-0.3°$. At this moment, the MTC force of plantar flexor was decreased and the MTC force of dorsiflexor was increased, so the exoskeleton generates forward rotation assistance ankle torque to reflect on the forward rotation torque led by wearer's gravity change and the wearer gradually stabilised at the equilibrium position around $-2.9° \sim -2.8°$. Conversely, when the vehicle was provided a negative acceleration at time point 30s, the wearer leaned forward, in reference to the equilibrium position, to about $-4.7°$. The corresponding change of the wearer's gravity led to some forward rotation torque, and the exoskeleton reacted on this by producing appropriate backward rotation torque. That is, the MTC force of plantar flexor was increased and the MTC force of dorsiflexor was decreased. These forces worked together to take the wearer to the equilibrium position around $-2.9° \sim -2.8°$.

C. PERSONALIZED EXOSKELETON CONTROL FOR DIFFERENT WEARERS

This simulation utilized a varied human model, i.e., the Variant Model, as shown in Table. 1 for the upright control to verify the adaptivity of proposed control strategy. Due to the change of the wearer model, the previous rule base will not be able to generate satisfied ankle torque. Therefore, the rule base would be updated based on the rule revision mechanism which is detailed in Section III-C.3. In particular, the weights of the dated rules would be decreased along time, and finally be gradually excluded form the rule base; also, high quality newly interpolated rules will be included in the rule base. Along with the evolving of the PMG-FRI and DMG-FRI rule bases, the exoskeleton performed increasingly better.

When the wearer stood on the static platform, the overall tilt angle along with the evolving progress of the rule base are illustrated in Fig. 11. From this figure, it is clear that the wearer cannot stood upright in the beginning using the rule base developed for the "standard human" model. After 2000 performance iterations, the revised rules base enabled the wearer to gradually stabilise at around $-5.9°$; at this point, the stabilised forward angle was larger than the human stabilised equilibrium position [43]. After 4000 performance iterations, the rule base enabled the wearer to gradually stabilise at around $-3.3°$, which was still larger than the normal human stabilised equilibrium position. The rule bases are stabilised after 6000 performance iterations; the wearer at this point stabilised at around $-2.7° \sim -2.8°$, which was consistent with the human stabilised equilibrium position. A snapshot of the rule base after 6000 performance iterations is summarised in Table 5.

After the rule base was stabilized for the Variant Model on a static platform, the next experiment was made on a moving vehicle, and the vehicle moving process was the same with that as introduced in Section IV-B. The simulation results regarding human body tilt angle, each flexor MTC force, and the ankle torque are illustrated in Fig. 12. Compared with

TABLE 5. The random snapshot of the evolved rule base for plantar flexor MTC model of "Individual Human".

E-FRI	i	A_i	B_i	w_i	EF_i	CD_i
PMG-FRI	1	$(74, 98, 139)$	$(0.029, 0.035, 0.046)$	0.209	341	63
	2	$(158, 231, 273)$	$(0.051, 0.069, 0.081)$	0.223	366	238
	3	$(281, 312, 366)$	$(0.083, 0.091, 0.106)$	0.251	410	16
	4	$(430, 502, 502)$	$(0.013, 0.028, 0.037)$	0.419	716	47
DMG-FRI	1	$(26, 102, 141)$	$(0.020, 0.049, 0.064)$	0.165	268	152
	2	$(125, 202, 245)$	$(0.058, 0.088, 0.104)$	0.208	338	31
	3	$(280, 324, 376)$	$(0.118, 0.135, 0.156)$	0.195	317	80
	4	$(460, 533, 563)$	$(0.191, 0.221, 0.233)$	0.368	619	0

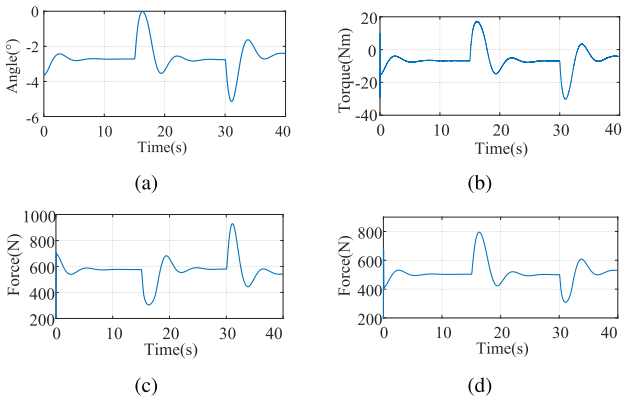

FIGURE 12. Simulation results of robotic ankle exoskeleton for upright balance control on the moving vehicle for the Variant Human Model. (a) Body tilt angle. (b) Ankle torque. (c) Plantar Flexor MTC Force. (d) Dorsiflexor MTC Force.

the simulation results as reported in Section IV-B based on the Standard Human Model, the tilt range in this experiment was wider for the Variant Model due to bigger body size, and accordingly larger assistance ankle torque was required to restore the equilibrium position for the wearer. In particular, the wearer leaned forward approximately $-3.7°$, and the robotic ankle exoskeleton assisted the wearer to lean backward to about $-2.5°$; and then the body gradually stabilised at around $-2.9° \sim -2.8°$, which is consistent with the result as reported in [43]. As the vehicle imposed acceleration (either positive or negative), the wearer gradually satbilised at the equilibrium position around $-3° \sim -2.8°$. Compared with the equilibrium position, the maximum leaned backward position was $-0°$ and maximum leaned forward position was about $-5.2°$. The MTC force of plantar flexor and dorsiflexor worked together to take the wearer to the equilibrium position, with the same process as discussed in Section IV-B.

D. PERSONALIZED CONTROL FOR DIFFERENT WEARERS WITH VARIOUS NEEDS

The assistance ankle torque demands can vary for different purposes, such as the needs at different rehabilitation treatment stages. To verify the power of the proposed approach in dealing with this situation, this experiment assumed that the wearer's two ankle muscle groups were activated as 0.2 and

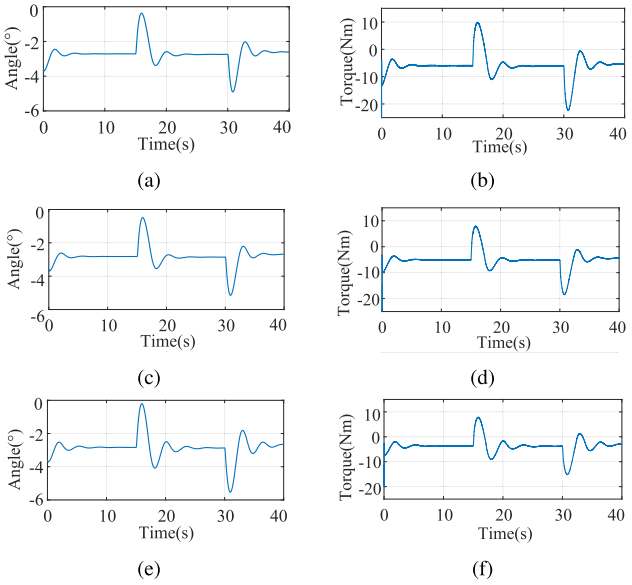

FIGURE 13. Simulation results based on different support needs. (a) Body tilt angle as wearer muscle activation degree is 0. (b) Provide assistance ankle torque as wearer muscle activation degree is 0. (c) Body tilt angle as wearer muscle activation degree is 0.2. (d) Provide assistance ankle torque as wearer muscle activation degree is 0.2. (e) Body tilt angle as wearer muscle activation degree is 0.4. (f) Provide assistance ankle torque as wearer muscle activation degree is 0.4.

TABLE 6. The random snapshot of the evolved rule base as wearer's muscle activation degree is 0.2.

E-FRI	i	A_i	B_i	w_i	EF_i	CD_i
PMG-FRI	1	$(252, 308, 372)$	$(0.071, 0.085, 0.103)$	0.171	277	50
	2	$(352, 396, 463)$	$(0.097, 0.108, 0.126)$	0.225	412	545
	3	$(530, 560, 617)$	$(0.144, 0.151, 0.168)$	0.110	193	109
	4	$(19, 83, 117)$	$(0.013, 0.028, 0.037)$	0.280	497	48
DMG-FRI	1	$(206, 232, 294)$	$(0.069, 0.077, 0.096)$	0.125	202	5
	2	$(327, 365, 399)$	$(0.106, 0.118, 0.129)$	0.242	395	64
	3	$(412, 462, 496)$	$(0.134, 0.149, 0.161)$	0.165	267	41
	4	$(549, 636, 683)$	$(0.177, 0.205, 0.221)$	0.267	439	48

0.4 compared with those of normal people, to simulate two different stages of rehabilitation treatment. The rule base revision process was the same as discussed above. A sample of the revised rule bases in this simulation are illustrated in Tables 6 and 7. Based on these rule bases, the robotic ankle exoskeleton could assist the wearer to achieve upright balance rehabilitation treatment on a moving platform.

In this simulation, the accelerating process of the vehicle is the same with that as discussed in Section IV-B. In order to facilitate the comparison, the wearer's body tilt angle and the corresponding exoskeleton assistance ankle torque are illustrated in Fig. 13. From this figure, it can be seen that the change trends of the wearer body tilt angles are very similar for different levels of support, but the magnitudes are significantly different. In specific, the exoskeleton assistance ankle torque decreased due to the muscle activation degree increased. This is reasonable as the wearer's muscle was

TABLE 7. The random snapshot of the evolved rule base as wearer's muscle activation degree is 0.4.

E-FRI	i	A_i	B_i	w_i	EF_i	CD_i
PMG-FRI	1	$(157, 228, 275)$	$(0.045, 0.062, 0.072)$	0.184	298	110
	2	$(366, 426, 476)$	$(0.095, 0.109, 0.121)$	0.214	349	84
	3	$(495, 544, 598)$	$(0.127, 0.135, 0.153)$	0.216	351	21
	4	$(589, 664, 708)$	$(0.149, 0.169, 0.181)$	0.289	476	53
DMG-FRI	1	$(122, 157, 233)$	$(0.036, 0.044, 0.063)$	0.177	286	10
	2	$(255, 324, 365)$	$(0.068, 0.086, 0.096)$	0.131	211	20
	3	$(358, 420, 451)$	$(0.094, 0.110, 0.118)$	0.204	332	35
	4	$(587, 621, 660)$	$(0.154, 0.163, 0.173)$	0.251	410	16

activated which could offer force to support the moments when the body fell down, which therefore effectively implemented the personalized support of robotic ankle exoskeleton, based on the individual's needs.

V. CONCLUSION

Personalized control plays a key role to promote the development and utilization of robotic exoskeletons. This paper proposes an adaptive control system for the robotic ankle exoskeleton, which is able to adaptively meet wearer's individual needs. The control system is implemented by utilizing experience-base FRI with the support of a MTC model, which is able to adaptively evolve the rule base based on the feedback collected from the wearer. The experimental results based on different human models with various support demands demonstrated the power of the proposed control system in improving the adaptability of robotic ankle exoskeleton. This is of high pragmatic and financial interest towards the commercial production of robotic ankle exoskeleton in mass volume for personalized use but without considering the differences between individuals during production. Although the proposed system in this paper only targets the ankle exoskeleton, it is readily applicable to the whole body exoskeleton, which remains as a piece of future work. In addition, further work is also required to apply the proposed control system to physical exoskeletons for extended evaluation, in addition to the simulation-based experiments as reported in this paper.

REFERENCES

[1] M. Vukobratovic, D. Hristic, and Z. Stojiljkovic, "Development of active anthropomorphic exoskeletons," *Med. Biol. Eng.*, vol. 12, no. 1, pp. 66–80, Jan. 1974.
[2] A. Agrawal, O. Harib, A. Hereid, S. M. Masselin, L. Praly, A. D. Ames, K. Sreenath, and J. W. Grizzle, "First steps towards translating HZD control of bipedal robots to decentralized control of exoskeletons," *IEEE Access*, vol. 5, pp. 9919–9934, 2017.
[3] A. Esquenazi, M. Talaty, and A. Jayaraman, "Powered exoskeletons for walking assistance in persons with central nervous system injuries: A narrative review," *PM&R*, vol. 9, no. 1, pp. 46–62, Jan. 2017.
[4] D. A. Winter, "Human balance and posture control during standing and walking," *Gait & posture*, vol. 3, no. 4, pp. 193–214, Dec. 1995.
[5] B. I. Han, H. S. Song, and J. S. Kim, "Vestibular rehabilitation therapy: Review of indications, mechanisms, and key exercises," *J. Clin. Neurol.*, vol. 7, no. 4, pp. 184–196, Dec. 2011.
[6] A. S. Pollock, B. R. Durward, P. J. Rowe, and J. P. Paul, "What is balance?" *Clin. Rehabil.*, vol. 14, no. 4, pp. 402–406, Aug. 2000.
[7] P. Gatev, S. Thomas, T. Kepple, and M. Hallett, "Feedforward ankle strategy of balance during quiet stance in adults," *J. Physiol.*, vol. 514, no. 3, pp. 915–928, Feb. 1999.
[8] K. Yin, M. Pang, K. Xiang, J. Chen, and S. Zhou, "Fuzzy iterative learning control strategy for powered ankle prosthesis," *Int. J. Intell. Robot. Appl.*, vol. 2, no. 1, pp. 122–131, Mar. 2018.
[9] J. M. Caputo and S. H. Collins, "A universal ankle–foot prosthesis emulator for human locomotion experiments," *J. Biomech. Eng.*, vol. 136, no. 3, Feb. 2014, Art. no. 035002.
[10] H. Geyer and H. Herr, "A muscle-reflex model that encodes principles of legged mechanics produces human walking dynamics and muscle activities," *IEEE Trans. Neural Syst. Rehabil. Eng.*, vol. 18, no. 3, pp. 263–273, Jun. 2010.
[11] R. W. Jackson and S. H. Collins. (2017). *Heuristic-Based Online Adaptation of Ankle Exoskeleton Assistance Using Plantarflexor Electromyography*. [Online]. Available: http://biomechatronics.cit.cmu.edu/publications.html
[12] B. Ugurlu, C. Doppmann, M. Hamaya, P. Forni, T. Teramae, T. Noda, and J. Morimoto, "Variable ankle stiffness improves balance control: Experiments on a bipedal exoskeleton," *IEEE/ASME Trans. Mechatronics*, vol. 21, no. 1, pp. 79–87, Feb. 2016.
[13] V. Rajasekaran, J. Aranda, A. Casals, and J. L. Pons, "An adaptive control strategy for postural stability using a wearable robot," *Robot. Auto. Syst.*, vol. 73, pp. 16–23, Nov. 2015.
[14] V. Huynh, C. Bidard, and C. Chevallereau, "Balance control for an active leg exoskeleton based on human balance strategies," in *Proc. Int. Workshop Medical Service Robots*. Cham, Switzerland: Springer, 2016, pp. 197–211.
[15] J. Li, H. P. Shum, X. Fu, G. Sexton, and L. Yang, "Experience-based rule base generation and adaptation for fuzzy interpolation," in *Proc. IEEE Int. Conf. Fuzzy Syst. (FUZZ-IEEE)*. Jul. 2016, pp. 102–109.
[16] H. Geyer, A. Seyfarth, and R. Blickhan, "Positive force feedback in bouncing gaits?" *Proc. Roy. Soc. London B, Biol. Sci.*, vol. 270, no. 1529, pp. 2173–2183, Oct. 2003.
[17] A. L. Hof, B. A. Geelen, and J. Van den Berg, "Calf muscle moment, work and efficiency in level walking; Role of series elasticity," *J. Biomech.*, vol. 16, no. 7, pp. 523–537, 1983.
[18] A. V. Hill, "The heat of shortening and the dynamic constants of muscle," *Proc. Roy. Soc. London. Ser. B, Biol. Sci.*, vol. 126, no. 843, pp. 136–195, Oct. 1938.
[19] J. M. Wang, S. R. Hamner, S. L. Delp, and V. Koltun, "Optimizing locomotion controllers using biologically-based actuators and objectives," *ACM Trans. Graph.*, vol. 31, no. 4, p. 25, Jul. 2012.
[20] E. H. Mamdani, "Application of fuzzy logic to approximate reasoning using linguistic synthesis," in *Proc. 76th Int. Symp. Multiple-Valued Logic*, May 1976, pp. 196–202.
[21] Y. Tan, J. Li, M. Wonders, F. Chao, H. P. H. Shum, and L. Yang, "Towards sparse rule base generation for fuzzy rule interpolation," in *Proc. IEEE Int. Conf. Fuzzy Syst. (FUZZ-IEEE)*, Jul. 2016, pp. 110–117.
[22] L. Yang and Q. Shen, "Adaptive fuzzy interpolation," *IEEE Trans. Fuzzy Syst.*, vol. 19, no. 6, pp. 1107–1126, Dec. 2011.
[23] L. Yang, Z. Zuo, F. Chao, and Y. Qu, "Fuzzy interpolation systems and applications," in *Modern Fuzzy Control Systems and Its Applications*. Rijeka, Croatia: IntechOpen, 2017.
[24] L. Yang and Q. Shen, "Closed form fuzzy interpolation," *Fuzzy Sets Syst.*, vol. 225, pp. 1–22, Aug. 2013.
[25] Z. Huang and Q. Shen, "Fuzzy interpolation and extrapolation: A practical approach," *IEEE Trans. Fuzzy Syst.*, vol. 16, no. 1, pp. 13–28, Feb. 2008.
[26] C. Chen and N. Mac Parthaláin, Y. Li, C. Price, C. Quek, and Q. Shen, "Rough-fuzzy rule interpolation," *Inf. Sci.*, vol. 351, pp. 1–17, Jul. 2016.
[27] N. Naik, R. Diao, and Q. Shen, "Dynamic fuzzy rule interpolation and its application to intrusion detection," *IEEE Trans. Fuzzy Syst.*, vol. 26, no. 4, pp. 1878–1892, Aug. 2018.
[28] L. Yang and Q. Shen, "Towards adaptive interpolative reasoning," in *Proc. IEEE Int. Conf. Fuzzy Syst.*, Aug. 2009, pp. 542–549.
[29] L. Yang, F. Chao, and Q. Shen, "Generalized adaptive fuzzy rule interpolation," *IEEE Trans. Fuzzy Syst.*, vol. 25, no. 4, pp. 839–853, Aug. 2017.
[30] F. Di Nardo, A. Mengarelli, E. Maranesi, L. Burattini, and S. Fioretti, "Assessment of the ankle muscle co-contraction during normal gait: A surface electromyography study," *J. Electromyography Kinesiology*, vol. 25, no. 2, pp. 347–354, Apr. 2015.

[31] S.-M. Chen and S. I. Adam, "Weighted fuzzy interpolated reasoning based on ranking values of polygonal fuzzy sets and new scale and move transformation techniques," *Inf. Sci.*, vol. 435, pp. 184–202, Apr. 2018.
[32] K. Balázs and L. T. Kóczy, "Hierarchical-interpolative fuzzy system construction by genetic and bacterial programming algorithms," in *Proc. IEEE Int. Conf. Fuzzy Syst. (FUZZ-IEEE)*, Jul. 2011, pp. 2116–2122.
[33] S.-M. Chen and S. I. Adam, "Adaptive fuzzy interpolation based on ranking values of interval type-2 polygonal fuzzy sets," *Inf. Sci.*, vol. 435, pp. 320–333, Apr. 2018.
[34] B. Bouchon-Meunier and L. Valverde, "A fuzzy approach to analogical reasoning," *Soft Comput.*, vol. 3, no. 3, pp. 141–147, Nov. 1999.
[35] A. Idri, I. Abnane, and A. Abran, "Missing data techniques in analogy-based software development effort estimation," *J. Syst. Softw.*, vol. 117, pp. 595–611, Jul. 2016.
[36] S. Salahshour and T. Allahviranloo, "Application of fuzzy differential transform method for solving fuzzy volterra integral equations," *Appl. Math. Model.*, vol. 37, no. 3, pp. 1016–1027, Feb. 2013.
[37] Z. Huang and Q. Shen, "Fuzzy interpolative reasoning via scale and move transformations," *IEEE Trans. Fuzzy Syst.*, vol. 14, no. 2, pp. 340–359, Apr. 2006.
[38] Q. Shen and L. Yang, "Generalisation of scale and move transformation-based fuzzy interpolation," *J. Adv. Comput. Intell. Intell. Inform.*, vol. 15, no. 3, pp. 288–298, 2011.
[39] S.-J. Chen and S.-M. Chen, "Fuzzy risk analysis based on similarity measures of generalized fuzzy numbers," *IEEE Trans. Fuzzy Syst.*, vol. 11, no. 1, pp. 45–56, Feb. 2003.
[40] S. L. Delp, F. C. Anderson, A. S. Arnold, P. Loan, A. Habib, C. T. John, E. Guendelman, and D. G. Thelen, "OpenSim: Open-source software to create and analyze dynamic simulations of movement," *IEEE Trans. Biomed. Eng.*, vol. 54, no. 11, pp. 1940–1950, Nov. 2007.
[41] S. R. Hamner, A. Seth, and S. L. Delp, "Muscle contributions to propulsion and support during running," *J. Biomech.*, vol. 43, no. 14, pp. 2709–2716, Oct. 2010.
[42] S. R. Hamner and S. L. Delp, "Muscle contributions to fore-aft and vertical body mass center accelerations over a range of running speeds," *J. Biomech.*, vol. 46, no. 4, pp. 780–787, Feb. 2013.
[43] M. Pang, M. Li, K. Xiang, and Y. Ge, "Human ankle joint reflex and impedance control during upright stance balance," *Huazhong Univerisity Sci. Technol.*, vol. 45, no. 10, pp. 49–53, Oct. 2017.

KAIYANG YIN received the M.E. degree from the Wuhan University of Technology, Wuhan, China, in 2015, where he is currently pursuing the Ph.D. degree. He is also a Visiting Ph.D. Student with the Department of Computer and Information Sciences, Northumbria University, Newcastle upon Tyne, U.K. His research interests include human motion signal analysis, bipedal robots control, and fuzzy logic systems.

KUI XIANG received the B.E. degree from the Wuhan Technical University of Surveying and Mapping, Wuhan, China, in 1999, and the M.E. degree in mechanical dynamics and the Ph.D. degree in system sciences from Zhejing University, Hangzhou, China, in 2002 and 2006, respectively. He is currently a Full Professor with the School of Automation, Wuhan University of Technology, Wuhan, China. His research interests include human motion signal analysis, modeling and statistical learning, and bipedal robots design and control.

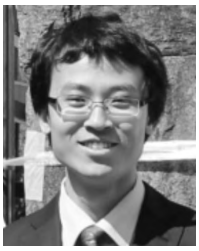

MUYE PANG received the Ph.D. degree in intelligent mechanical engineering from Kagawa University, Kagawa, Japan, in 2015. He is currently an Associate Professor with the School of Automation, Wuhan University of Technology, Wuhan, China. His research interests include bipedal robot, push recovery, muscle reflex, and surface electromyographic signal.

JING CHEN received the B.E. degree from the Huazhong University of Science and Technology, Wuhan, China, in 1990, and the M.E. degree in industry automation and the Ph.D. degree in vibration control of civil engineering structure from the Wuhan University of Technology, Wuhan, China, in 1997 and 2003, respectively, where she is currently a Full Professor with the School of Automation. Her research interests include control science and engineering and computer control.

PHILIP ANDERSON received the B.Sc. degree from Northumbria University, U.K., in 1997, and the M.Sc. degree in distance education from Athabasca University, Canada. He is currently a Senior Lecturer with the Department of Computer and Information Sciences, Northumbria University. His research interests include digital forensics (computer and mobile devices), information security (frameworks, good governance, and risk management), and incident response (detecting, reporting, and handling). His current research focuses on the use of machine learning techniques to develop intelligent grooming detection systems.

LONGZHI YANG (M'12–SM'17) received the B.Sc. degree from the Nanjing University of Science and Technology, Nanjing, China, in 2003, the M.Sc. degree from Coventry University, Coventry, U.K., in 2006, and the Ph.D. degree from Aberystwyth University, Aberystwyth, U.K., in 2011, all in computer science. He is currently the Director of Learning and Teaching and an Associate Professor with the Department of Computer and Information Sciences, Northumbria University, U.K. His research interests include computational intelligence, machine learning, big data, computer vision, intelligent control systems, robotics, and the applications of such techniques under real-world uncertain environment. He is the Founding Chair of the IEEE Special Interest Group on Big Data for Cyber Security and Privacy. He received the Best Student Paper Award at the 2010 IEEE International Conference on Fuzzy Systems.